Published in final edited form as:
Nature. 2014 April 24; 508(7497): 541–545. doi:10.1038/nature13079.

Cell-cycle-regulated activation of Akt kinase by phosphorylation at its carboxyl terminus

Pengda Liu[1], **Michael Begley**[2,3], **Wojciech Michowski**[4], **Hiroyuki Inuzuka**[1], **Miriam Ginzberg**[5], **Daming Gao**[1], **Peiling Tsou**[2,3], **Wenjian Gan**[1], **Antonella Papa**[1,2,6], **Byeong Mo Kim**[8], **Lixin Wan**[1], **Amrik Singh**[7], **Bo Zhai**[5], **Min Yuan**[2], **Zhiwei Wang**[1,†], **Steven P. Gygi**[5], **Tae Ho Lee**[8], **Kun-Ping Lu**[2], **Alex Toker**[1], **Pier Paolo Pandolfi**[1,2,6], **John M. Asara**[2], **Marc W. Kirschner**[3], **Piotr Sicinski**[4], **Lewis Cantley**[2,3,†], and **Wenyi Wei**[1]

[1]Department of Pathology, Beth Israel Deaconess Medical Center, Harvard Medical School, Boston, Massachusetts 02215, USA.

[2]Department of Medicine, Beth Israel Deaconess Medical Center, Boston, Massachusetts 02215, USA.

[3]Department of Systems Biology, Harvard Medical School, Boston, Massachusetts 02115, USA.

[4]Department of Cancer Biology, Dana-Farber Cancer Institute and Department of Genetics, Harvard Medical School, Boston, Massachusetts 02115, USA.

[5]Department of Cell Biology, Harvard Medical School, Boston, Massachusetts 02115, USA.

[6]Cancer Genetics Program and Division of Genetics, Department of Medicine, Beth Israel Deaconess Medical Center, Boston, Massachusetts 02115, USA.

[7]Cell Signaling Technology, Danvers, Massachusetts 01923, USA.

[8]Division of Gerontology, Department of Medicine, Beth Israel Deaconess Medical Center, Boston, Massachusetts 02215, USA.

Abstract

Akt, also known as protein kinase B, plays key roles in cell proliferation, survival and metabolism. Akt hyperactivation contributes to many pathophysiological conditions, including human cancers[1–3], and is closely associated with poor prognosis and chemo- or radio-therapeutic

†Present addresses: The Cyrus Tang Hematology Center, Jiangsu Institute of Hematology, the First Affiliated Hospital, Soochow University, Suzhou 215123, China (Z.W.); Cancer Center at Weill Cornell Medical College and NewYork-Presbyterian Hospital, New York, New York 10065, USA (L.C.).

Supplementary Information is available in the online version of the paper.

Author Contributions P.L., M.B., W.M., H.I., A.P., M.G., D.G., P.T. and W.G. performed most of the experiments with assistance from B.K., L.W., A.S., B.Z. and M.Y. W.W., P.S., P.P.P., L.C. and P.L. designed the experiments. W.W., L.C., P.S., P.P.P., M.W.K. and A.T. supervised the study. P.L. and W.W. wrote the manuscript. All authors commented on the manuscript.

Author Information Reprints and permissions information is available at www.nature.com/reprints. The authors declare no competing financial interests. Readers are welcome to comment on the online version of the paper. Correspondence and requests for materials should be addressed to W.W. (wwei2@bidmc.harvard.edu).

Online Content Any additional Methods, Extended Data display items and Source Data are available in the online version of the paper; references unique to these sections appear only in the online paper.

resistance[4]. Phosphorylation of Akt at S473 (ref. 5) and T308 (ref. 6) activates Akt. However, it remains unclear whether further mechanisms account for full Akt activation, and whether Akt hyperactivation is linked to misregulated cell cycle progression, another cancer hallmark[7]. Here we report that Akt activity fluctuates across the cell cycle, mirroring cyclin A expression. Mechanistically, phosphorylation of S477 and T479 at the Akt extreme carboxy terminus by cyclin-dependent kinase 2 (Cdk2)/cyclin A or mTORC2, under distinct physiological conditions, promotes Akt activation through facilitating, or functionally compensating for, S473 phosphorylation. Furthermore, deletion of the cyclin A2 allele in the mouse olfactory bulb leads to reduced S477/T479 phosphorylation and elevated cellular apoptosis. Notably, cyclin A2-deletion-induced cellular apoptosis in mouse embryonic stem cells is partly rescued by S477D/T479E-Akt1, supporting a physiological role for cyclin A2 in governing Akt activation. Together, the results of our study show Akt S477/T479 phosphorylation to be an essential layer of the Akt activation mechanism to regulate its physiological functions, thereby providing a new mechanistic link between aberrant cell cycle progression and Akt hyperactivation in cancer.

Using single live-cell imaging[8], we found that Akt activation fluctuated across the cell cycle, inversely correlating with Cdt1 abundance[9] (Fig. 1a and Supplementary Fig. 1a). Statistical analysis of immunostained HeLa cells further showed that Akt-pS473 has a similar periodic feature as geminin[9,10] (Fig. 1b). Notably, in several cancer cell lines (Fig. 1c, d and Supplementary Fig. 1b, c), Akt phosphorylation, but not total Akt abundance, fluctuated across the cell cycle. The periodic Akt phosphorylation mirrored the expression pattern of cyclin A2, the predominant mammalian cyclin A isoform[11], during cell cycle progression (Fig. 1c, d). Moreover, acute depletion of cyclin A2 or Cdk2, but not cyclin E, resulted in decreased Akt phosphorylation, with no significant impact on phosphorylation of Akt upstream kinases PDK1 and mTORC2 (Fig. 1d). This prompted us to evaluate whether Cdk2/cyclin A directly regulates Akt activation in a phosphorylation-dependent manner during the cell cycle[12].

In support of Akt as a Cdk2/cyclin A substrate, Akt isoforms interacted with cyclin A2 (Fig. 2a and Supplementary Fig. 2a). Furthermore, we identified four ‘RXL’ cyclin A-binding motifs[13] in Akt1 (Fig.2b), all of which are evolutionarily conserved (Supplementary Fig. 2b). Mutation of R76CL or R273DL, and to a lesser extent, R200VL or R370TL (RXL to AXA) attenuated Akt1 interaction with cyclin A2 (Fig. 2c), and reduced Akt1 activity (Supplementary Fig. 2c). Consistently, depleting cyclin A2 or Cdk2 (Supplementary Fig. 2d–f) led to a significant reduction in Akt phosphorylation. More importantly, either acute treatment with Cdk2 inhibitors (Fig. 2d) or deletion of the cyclin A2 allele in cyclin $A2^{f/f}$ primary mouse embryonic fibroblasts (MEFs) (Fig. 2e) led to a marked decrease in Akt phosphorylation without a significant perturbation of cell cycle progression (Fig. 2d and ref. 14), excluding a possible indirect cell cycle effect on Akt phosphorylation by inhibiting Cdk2/cyclin A.

Notably, deletion of cyclin A2, but not cyclin A1 or cyclin E1/E2 alleles, caused a significant decrease of Akt phosphorylation (Fig. 2f, g), whereas conversely, ectopic expression of cyclin A2 (Fig. 2h and Supplementary Fig. 3a) resulted in elevated Akt phosphorylation coupled with enhanced *in vitro* anchorage-independent growth

(Supplementary Fig. 3b, c). Moreover, depletion of Cdh1, the E3 ligase that controls cyclin A turnover[15], resulted in increased cyclin A2 abundance and elevated Akt phosphorylation, leading to enhanced *in vitro* anchorage-independent growth (Supplementary Fig. 3d, e) and *in vivo* tumour formation (Fig. 2i and Supplementary Fig. 3f–h). More importantly, increased Akt phosphorylation and tumor-igenicity by depleting Cdh1 could be partly reversed by extra depletion of cyclin A2 (Fig. 2j and Supplementary Fig. 3i–l). Collectively, these results support Cdk2/cyclin A2 as a major physiological kinase that governs Akt phosphorylation and oncogenic functions.

Notably, Cdk2/cyclin A directly phosphorylated Akt1 *in vitro* on its carboxy (C)-terminal region (Supplementary Fig. 4a, b). Serial truncations showed Cdk2/cyclin A phosphorylation sites in the last four evolutionarily conserved residues and subsequent mutageneses pinpointed both S477 and T479 as Cdk2/cyclin A sites (Supplementary Fig. 4c–e). Similarly, Cdk2/cyclin A phosphorylated Akt2-S478 (Supplementary Fig. 4f). Interestingly, mutation of G478 to proline (G478P) to mimic the canonical Cdk2 ‘SP/TP’ phospho-motif[16,17], or to other bulky amino acids (L/W/R), did not significantly affect Cdk2/cyclin-A-mediated Akt phosphorylation (Supplementary Fig. 4g). Conversely, C-terminal addition of an α-helix[18] (Supplementary Fig. 4g) or a green fluorescent protein (GFP) (Supplementary Fig. 4h) reduced Cdk2/cyclin-A-mediated phosphorylation of the engineered non-tail version of S477G478-, but not S477P478-Akt1. These data indicate that S477/T479 may belong to a new class of Cdk2/cyclin A phospho-motifs where relative structural flexibility at the Akt1 C terminus might override the requirement of an adjacent proline for Cdk2-mediated phosphorylation of canonical TP/SP sites[16,17] typically buried within defined structures.

Furthermore, mass spectrometry analyses confirmed Akt1 S477 and T479 phosphorylation[19] (Supplementary Fig. 5a–d). To gain further mechanistic insights, we developed phospho-specific antibodies that recognize pS477/pT479-Akt1 (Supplementary Fig. 6a–f), pS477-Akt1 or pT479-Akt1 (Supplementary Fig. 7a–h) *in vivo*. Owing to the large consistency among three antibodies under our experimental conditions, we focused on examining the correlation of Akt1-pS477/pT479 and Akt activation in the remainder of the studies. As with pS473-Akt1, Akt1 tail phosphorylation fluctuated during the cell cycle (Fig. 1c, d and Supplementary Fig. 1b, c), and was subjected to regulation by Cdk2/cyclin A (Fig. 2d–h). Furthermore, a positive correlation between cyclin A2 expression and Akt1-pS477/pT479 was observed in breast cancer patient samples (Fig. 2k and Supplementary Fig. 8a, b). More importantly, similar to the reported phosphorylation of Akt-S473 by several upstream kinases dependent on upstream stimuli[5,20,21], Akt1-pS477/pT479 could be mediated by mTOR (Supplementary Figs 9a–c, 10a–g and 11a–c) or DNAPK (Supplementary Fig. 9d, e), in addition to Cdk2/cyclin A. In keeping with this notion, elevated Akt1-pS477/pT479 was detected in *Pten* heterozygous MEFs (Supplementary Fig. 10h). Interestingly, Akt1-pS477/pT479 was negatively regulated by PTEN in mice in a tissue-specific manner and largely with Akt-pS473 (Supplementary Fig. 10i).

Moreover, inactivation of mTORC2 by depleting Rictor led to a more dramatic reduction of Akt1-pS477/pT479 in response to insulin (Supplementary Fig. 11a) than under synchronized cell cycle conditions (Supplementary Fig. 12a). Conversely, depletion of Cdk2, but not

Rictor (Supplementary Fig. 12a, b), resulted in a more robust reduction in Akt1-pS477/pT479 across the cell cycle. These findings suggest that Akt1-pS477/pT479 is possibly mediated by Cdk2/cyclin A, mTORC2 or DNAPK, under cell cycle progression, growth factor stimulation or DNA damaging conditions, respectively (Supplementary Fig. 13a, b). Notably, depletion of Cdk2, cyclin A2 or Rictor in human primary foreskin fibroblasts all resulted in reduced Akt1-pS477/pT479 (Supplementary Fig. 14a–c), highlighting both Cdk2/cyclin A and mTORC2 as upstream physiological kinases governing Akt1-pS477/pT479. We therefore next evaluated the contribution of Akt1-pS477/pT479 to Akt kinase activation under various cellular conditions.

In keeping with the notion that Akt1 tail phosphorylation is required to achieve full Akt1 activation, the phospho-deficient Akt1-S477A/T479A (Akt1-AA) mutant showed a dramatic suppression, whereas a phosphomimetic S477D/T479E (Akt1-DE) mutant showed enhanced Akt1 phosphorylation and activation (Fig. 3a–c and Supplementary Fig. 15a–c). However, caution needs to be taken in interpreting these results, as these mutations might not fully recapitulate the *in vivo* phosphorylation status. Strikingly, Akt1-AA was defective in pS473 even in the myristoylation-tagged constitutively active Akt1 (Fig. 3d), advocating a critical role for Akt1-pS477/pT479 in activating Akt (Supplementary Fig. 16a–c). Consistently, S477D/T479E effectively rescued Akt-pS473 and kinase activity of the cyclin A binding motif-defective mutant, R76A (Fig. 3e, f), as well as its anchorage-independent growth ability (Supplementary Fig. 16d). However, the rescue effect of DE on Akt1-R76A was not due to changes in its affinity with PIP3 (Supplementary Fig. 16e).

Consistent with S477/T479 being Cdk2/cyclin A sites, ectopic expression of Akt1-DE partly rescued cell cycle defects observed in quadruple knockout MEFs (cyclin $E1^{-/-}$/cyclin $E2^{-/-}$/cyclin $A1^{-/-}$/cyclin $A2^{f/f}$) after Cre infection (Fig. 3g and Supplementary Fig. 16f). Compared with the periodic phosphorylation of wild-type Akt1 (Akt1-WT), Akt1-AA was severely impaired, whereas Akt1-DE showed an elevated and constitutive S473/T308 phosphorylation across the cell cycle (Fig. 3h). More importantly, under several physiological conditions (Supplementary Fig. 17a–c), Akt-pS473/pT308 was severely compromised in Akt1-AA, but robustly elevated in Akt1-DE expressing cells. Consistently, depletion of cyclin A2 in Akt1-WT, but not Akt1-DE expressing cells, led to a significant reduction in Akt phosphorylation (Supplementary Fig. 17d) and decreased tumour formation *in vivo* (Fig. 3i and Supplementary Fig. 17e–g). Cumulatively, these data demonstrate that in response to several upstream signals, phosphorylation of Akt1-S477/T479 may govern the canonical Akt-pS473 to promote Akt activation. Thus, we next evaluated the precise molecular mechanism(s) linking Akt1-pS477/pT479 to pS473 and subsequent Akt activation.

As Akt2 crystal structures are reported in great detail[22,23], we next focused on understanding how Akt2-pS478 (equivalent to Akt1-pS477; Supplementary Figs 4d and 18a) modulates Akt2 kinase activity. Notably, Akt2-pS478 functioned synergistically with Akt2-pS474 (equivalent to Akt1-pS473) to allosterically activate Akt2 (Fig. 4a and Supplementary Fig. 18b). Mechanistically, Akt2-pS478 may create a new charge–charge interaction between S478D and R208 to stabilize Akt2 in its closed, active form (Supplementary Fig. 18c, d). Consistently, deletion of the Akt1-tail after amino acid 475 (termed 476Δ) led to

significantly increased Akt phosphorylation (Supplementary Fig. 18e), suggesting that either phosphorylation or deletion of the tail region could lock Akt in its active conformation.

Intriguingly, in addition to stabilizing Akt, Akt tail phosphorylation may alter Akt kinase kinetics to accelerate the kinase reaction (Supplementary Fig. 18f). Furthermore, pS473 and pS477/pT479, both of which activate Akt, are intrinsically linked; as compared with Akt1-WT, Akt1-DE but not Akt1-AA was preferentially phosphorylated by mTOR *in vitro* (Supplementary Fig. 19a, b). This indicates that pS477/pT479 might prime Akt1 for mTORC2-mediated phosphorylation of S473 (refs 5, 24) (Fig. 4b). Mechanistically, enhanced phosphorylation of Akt1-DE at S473 by mTOR may be in part due to its increased interaction with Sin1 (Fig. 4c) and mTOR, but not due to changes in its association with the Akt inhibitor CTMP[25] or phosphatase PHLPP2 (ref. 26) (Supplementary Fig. 19c, d). However, phospho-mimetic mutation of S473 (S473D) (Supplementary Fig. 20a) or its mimicking peptide library (Supplementary Fig. 20b) led to reduced Akt1 tail phosphorylation, suggesting that the pS477/pT479 event may precede pS473.

Mutation of either S473 or S477/T479 to alanine significantly reduced Akt activity towards phosphorylating Skp2 or crosstides, whereas no significant additive effect was observed in S473A/S477A/T479A (Supplementary Fig. 21a, b), arguing for a possible functional redundancy between pS477/pT479 and pS473 for Akt catalytic activity. Consistently, Akt1-DE kinase activity was largely unchanged after depletion of Rictor (Supplementary Fig. 21c, d), whereas Akt1-DE partly rescued the deficient Akt kinase activity in Akt1-S473A (Supplementary Fig. 21e, f). Given the close proximity of S473 and S477/T479, these results indicate that in addition to promoting pS473, pS477/pT479 may also trigger Akt activation independently of, or partly compensate for, pS473.

Biologically, phosphorylation of the Akt1 tail activated Akt1, leading to elevated Skp2 or FOXO phosphorylation, which further promoted cell cycle progression (Supplementary Fig. 22a–c), or conferred resistance to the chemotherapeutic agents etoposide or camptothecin (Supplementary Fig. 22d, e), respectively. More importantly, compared with Akt1-WT, Akt1-DE-expressing cells showed growth advantage in both *in vitro* soft agar (Fig. 4d, e) and *in vivo* tumour formation (Fig. 4f, g and Supplementary Fig. 23a, b) assays, supporting a role for Akt1-pS477/pT479 in promoting Akt1 activation and signalling phenotypes associated with malignancy. Notably, Akt1-476Δ phenocopied Akt1-DE by showing elevated Akt phosphorylation (Supplementary Fig. 18e), probably through enhanced interaction with mTORC2 (Supplementary Fig. 24a), thereby promoting *in vitro* anchorage-independent growth and *in vivo* tumorigenesis (Supplementary Fig. 24 b–f).

To study the *in vivo* physiological significance of Cdk2/cyclin-A-mediated phosphorylation on Akt1-S477/T479 further, we generated brain-specific cyclin A2 knockout mice with nestin-Cre[27]. Interestingly, a significant reduction in Akt1-pS477/pT479 was observed in cyclin $A2^{\Delta/\Delta}$ olfactory bulbs coupled with elevated cleavage of caspase 3 (Fig. 4h), suggesting that Akt1-pS477/pT479 might be critical for cell survival in olfactory bulbs. Consistently, acute ablation of cyclin A2 in cyclin $A2^{f/f}$ mouse embryonic stem cells led to induced cellular apoptosis (Fig. 4i and Supplementary Fig. 25a, d), providing a possible explanation for previous findings that deleting cyclin A2 abolished embryonic stem cell

colony formation *in vitro*[14]. Furthermore, cyclin A2-deletion-induced elevation of cellular apoptosis in mouse embryonic stem cells could be partly rescued by expressing Akt1-DE, but not Akt1-AA (Fig. 4i, j and Supplementary Fig. 25), supporting the idea that cyclin A2 may govern cellular survival *in vivo* largely by promoting Akt activation.

To extend these findings and their clinical relevance to human pathophysiology, we observed a positive correlation between Akt1-pS477/pT479 and Akt1-pS473 in samples from patients with breast cancer and breast-cancer-derived cell lines (Supplementary Fig. 26a–e). Interestingly, high levels of pS477/pT479 occurred at a relatively higher rate than pS473 in an earlier breast cancer developmental stage (stage II) (Supplementary Fig. 26d), indicating that pS477/pT479 may serve as a better biomarker for early-stage breast cancer detection, although further investigations are warranted.

Taken together, our data unravel a new phosphorylation event on Akt1 at its extreme C-terminal residues, S477 and T479, to trigger Akt1 activation either through enhancing the association between Akt1 and mTORC2 to promote pS473, or by functionally compensating for pS473 to lock Akt1 in its active conformation. More importantly, our study directly couples Akt activity with cell cycle progression, two well-characterized hallmarks of human cancers[28–30]. In this regard, our data suggest that cyclin A2 overexpression might exert its physiological functions in part by directly phosphorylating and activating Akt to trigger its pro-survival and oncogenic functions.

METHODS

Plasmids

pcDNA3-HA-Akt1/Akt2/Akt3 and pcDNA3-Myr-HA-Akt1 constructs were obtained from A. Toker and described previously[31]; pcDNA3-HA-Akt1-S477A, pcDNA3-HA-Akt1-T479A, pcDNA3-HA-Akt1-S477A/T479A, pcDNA3-HA-Akt1-S477D, pcDNA3-HA-Akt1-S479E, pcDNA3-HA-Akt1-S477D/T479E, pcDNA3-HA-Akt2-S478A, pcDNA3-HA-Akt2-S478D, pcDNA3-HA-Akt3-S474A, pcDNA3-HA-Akt3-S474D, pcDNA3-Myr-HA-Akt1-S477A/T479A, pcDNA3-Myr-HA-Akt1-S477D/T479E, pcDNA3-HA-Akt1-R76LAA, pcDNA3-HA-Akt1-R76LAA/DE, pcDNA3-HA-Akt1-R200LAA, pcDNA3-HA-Akt1R273LAA, pcDNA3-HA-Akt1-R370LAA and pcDNA3-HA-Akt1-4A constructs, as well as the shAkt1-resistant versions of Akt constructs, were generated using a QuikChange XL Site-Directed Mutagenesis Kit (Stratagene) according to the manufacturer's instructions, with specific primer sequences available upon request. The various (glutathione *S*-transferase) GST–Akt1 plasmids used for *in vitro* kinase assays were constructed by sub-cloning corresponding PCR fragments into the pGEX-4T-1 vector by BamHI/EcoRI sites for amino (N)-terminal GST tag. pBabe-Myr-HA-Akt1-WT, S477A/T479A, S477D/T479E, R76A and R76A/DE retroviral vectors were generated by sub-cloning Akt1 from corresponding pcDNA3-Myr-HA-Akt1 vectors into the pBabe-HA-hygromycin vector or MSCV-hygromycin vector. Flag–Skp2 vector was constructed as described previously[31]. Cre adenoviruses were obtained from the laboratory of P.S. The phage-Cre construct was obtained from the laborator y of L. Glimcher. The Cre-ER construct was obtained from the laboratory of P. Pandolfi. The pTRIPZ-cyclin A2 was constructed by cloning the cyclin A2 allele into pTRIPZ vector by AgeI/ClaI sites. Akt activity reporter (Akt AR) was obtained

from J. Zhang as described previously[8]. Cdt1 and geminin fucci reporters were obtained from A. Miyawaki as described previously[9].

shRNAs and siRNAs

shRNA vectors to deplete endogenous Akt1 were described previously[31]. shRictor vectors were purchased from Addgene (1854). shRNA vectors to deplete endogenous Cdk2 were purchased from Open Biosystems (RHS4533-EG1017). shCdh1 and shPTEN vectors were described previously[32]. To generate the lentiviral shRNA constructs against human cyclin A2, the following sequences were cloned into the pLKO-puro vector (shCyclin A2 no. 1 sense: 5′-CCGGAAGGCAGCGCCCGTCCAACAACTCGAGTTGTTGGAGCGGCGCTGCCTTTTTTTG-3′; shCyclin A2 no. 1 anti-sense: 5′-AATTCAAAAAAAGGCAGCGCCCGTCCAACAACTCGAGTTGTTGGAGCGGCGCTGCCTT-3′; shCyclin A2 no. 2 sense: 5′-CCGGAACTACATTGATAGGTTCCTGCTCGAGCAGGAACGTATCAATGTAGTTTTTTTG-3′; shCyclin A2 no. 2 anti-sense: 5′-AATTCAAAAAAACTACATTGATAGGTTCCTGCTCGAGCAGGAACGTATCAATGTAGTT-3′). Cyclin A2, Akt1, Cdk2 and cyclin E siRNA oligonucleotides and the siRNA transfection method have been described previously[31].

Antibodies

Anti-Sin1 antibody for western blots was purchased from Millipore (07-2276). Anti-Akt1 antibody conjugated agarose beads for endogenous Akt1 immunoprecipitation were purchased from Cell Signaling Technology (3653S). Anti-mTOR antibody (2972), anti-pSer2481-mTOR antibody (2974), anti-Raptor antibody (2280), anti-Rictor antibody (9476), anti-phospho-Ser473-Akt antibody (4051), anti-phospho-Thr308-Akt antibody (2965), anti-phospho-Thr450-Akt antibody (9267), anti-Akt1 antibody (2938), anti-Akt total antibody (4691), anti-phospho-Thr389-S6K antibody (9205), anti-S6K antibody (9202), anti-phospho-Akt substrate (RxRxxpS/T) antibody (9614), anti-phospho-PDK1 antibody (3438), anti-phospho-TSC2-antibody (3617), anti-TSC2 antibody (3990), anti-phospho-T24/32-FOXO1/3a antibody (9464), anti-phospho-S253-FOXO 3a antibody (9466), anti-phospho-S256-FOXO1 antibody (9461), anti-FOXO1 antibody (2880), anti-FOXO3a antibody (2497), anti-phospho-pRAS40 (T246) antibody (2997), anti-pRAS40 antibody (2691), anti-Skp2 antibody (4313), anti-pS9-GSK3β antibody (9323), anti-GSK3β antibody (9315) and anti-Cdt1 antibody (8064) were purchased from Cell Signaling Technology. Anti-cyclin A2 (sc-751), anti-cyclin E (sc-247), anti-Cdk2, anti-cyclin B1 (sc-245) and polyclonal anti-HA antibody (sc-805) were purchased from Santa Cruz. Anti-geminin (ab12147) was purchased from Abcam. Anti-Tubulin antibody (T-5168), anti-Vinculin antibody (V-4505), polyclonal anti-Flag antibody (F-2425), monoclonal anti-Flag antibody (F-3165), anti-Flag agarose beads (A-2220), anti-HA agarose beads (A-2095), peroxidase-conjugated anti-mouse secondary antibody (A-4416) and peroxidase-conjugated anti-rabbit secondary antibody (A-4914) were purchased from Sigma. Monoclonal anti-HA antibody (MMS-101P) was purchased from Covance. Various anti-pS477-Akt1, anti-pT479-Akt1 and anti-pS477/pT479-Akt1 antibodies and the anti-pS72-Skp2 antibody were produced by Cell Signaling Technology.

Immunoblots and immunoprecipitation

Cells were lysed in EBC buffer (50 mM Tris pH 7.5, 120 mM NaCl, 0.5% NP-40) (for immunoprecipitation) supplemented with protease inhibitors (Complete Mini, Roche) and phosphatase inhibitors (phosphatase inhibitor cocktail set I and II, Calbiochem). The total protein concentrations of whole cell lysates were measured by a Beckman Coulter DU-800 spectrophotometer using the Bio-Rad protein assay reagent. The same amounts of whole cell lysates were resolved by SDS–PAGE and immunoblotted with indicated antibodies. For immunoprecipitation, 1000 μg lysates were incubated with the indicated antibody (1–2 μg) for 3–4 h at 4 °C followed by incubation for 1 h with Protein A Sepharose beads (GE Healthcare). Immunoprecipitants were washed five times with NETN buffer (20 mM Tris, pH 8.0, 100 mM NaCl, 1 mM EDTA, 0.5% NP-40) before being resolved by SDS–PAGE and immunoblotted with indicated antibodies.

Cell culture and cell viability assays

Cell culture and transfection procedures have been described previously[31,33]. The WT and *Akt1*$^{-/-}$/*Akt2*$^{-/-}$ MEFs were obtained from N. Hay as described previously[34]. Retroviral shRNA virus packaging and subsequent infection of various cell lines were performed according to the protocol described previously[35]. For cell viability assays, cells were plated at 10,000 per well in 96-well plates, and incubated with complete Dulbecco's Modified Eagle Medium (DMEM) medium containing different concentrations of etoposide (Sigma, E1383), camptothecin (Sigma C156) and doxorubicin (Sigma, D1515) for 48 h. Assays were performed with a CellTiter-Glo Luminescent Cell Viability Assay Kit according to the manufacturer's instructions (Promega).

Single-cell imaging

Single live-cell imaging procedures were done according to previously described methods[36] with some modifications as described below. Cells were plated on number 1.5 coverslips MatTek Dish (P35G-1.5-14-C). DMEM media (GIBCO) containing 25 mM HEPES, 25 mM glucose (except for the experiment of manipulating glucose concentration), 2 mM glutamine and 3% FBS (phenol red was excluded during image acquisition). Cells were imaged on a Nikon TE 2000E and a Nikon and Ti motorized inverted microscope with a 20×/0.75 or 60×/1.4 (oil immersion) numerical aperture objective lens. Dual emission ratio imaging was performed with a 436/10 filter, a diachronic mirror (Chroma 86002v1bs) and two emission filters (470/30 for cyan and 535/30 for yellow). All optical filters were obtained from Chroma Technologies. Images were acquired with a Hamamatsu ORCA-R2 cooled charge-coupled device (CCD) camera controlled with MetaMorph 7 software (Molecular Devices) and the Perfect Focus System for continuous maintenance of focus. Fluorescence images were background-corrected. For time-lapse experiments, images were collected every 30 min for 24 consecutive hours, with an exposure time of 50–100 ms and 2 × 2 binning, with illumination light shuttered between acquisitions. The ratios of yellow-to-cyan were then calculated at different time points and normalized by dividing all ratios by the emission ratio before stimulation, setting the basal emission ratio as 1.

Mapping the cell-cycle progression status in individual cells

The procedures for performing this experiment were as described previously[37]. Briefly, to relate the elapsed time after cell division to cell-cycle phase and progression with the abundance or activities of the proteins of interest, we measured the distribution of DNA content in an asynchronously growing culture by flow cytometry using propidium iodide staining, as well as the gemenin abundance by a GFP–gemenin reporter as described previously[9]. HeLa cells expressing the mAG-hGem fucci reporter system[9] were cultured in DMEM (Cellgro; DMEM 10-017-CV) with 10% FBS (Gibco; 26140) and 1% penicillin/streptomycin solution (Cellgro; 30-002-CI). Media were further supplemented with 3 μg ml^{-1} blasticidin (InvivoGen; ant-bl-5b) to maintain selection of cells expressing mAG-hGem. For experiments, cells were plated on 24 mm × 60mm coverslips, no. 1.5 (VWR; 48393-252). Before plating, coverslips were sterilized by incubation for 20 min in 70% ethanol at room temperature and then dried in sterile conditions. Cells were typically plated at 1×10^5 cells per millilitre in to 15 cm dishes that were pre-prepared with sterile coverslips as described above. Cells were fixed approximately 48 h after plating. The kinase activities of Akt were measured by anti-p-S473-Akt antibody. These distributions were fitted using a modification of the Dean–Jett model[38] to determine the number of cells in G1, S and G2 phases and were subsequently translated to the time spent in various cell-cycle phases using a previously published model[39].

Fixing and staining cells for immunofluorescence

To fix cells, coverslips were incubated for 10 min in 4% paraformaldehyde (Alfa Aesar, 30525-89-4) at room temperature. Cells were then permeabilized for 5 min in dry methanol at −20 °C and rehydrated in PBS. Cells were incubated with primary antibody (either Anti-phospho-Akt (S473) (Cell Signaling; 4060S) or Anti-Akt (Cell Signaling, 4060S)) overnight at 4 °C, followed by incubation with a fluorescent secondary antibody (Invitrogen, A-21429) for 1 h at room temperature. Antibody solutions were made in PBS with 2% bovine serum albumin (BSA). DNA was stained by incubating in 10 μM 4′,6-diamidino-2-phenylindole (DAPI) for 5 min. To label protein mass, fixed, permeabilized samples were incubated with 0.04 μg ml^{-1} succinimidyl ester linked dye diluted in PBS (Alexa Fluor 647 carboxylic acid, succinimidyl ester; Invitrogen, A-20106). Following labelling procedures, cells were mounted on glass slides in ProLong Gold antifade (Life Technologies, P36930).

Microscopy

Slides prepared as described above were imaged with a Nikon Ti inverted fluorescence microscope with Perfect Focus controlled by Nikon Elements. We used the scan-slide function to image the full area of the slide at ×20 magnification. The microscope was surrounded by a custom enclosure to maintain constant temperature and atmosphere. The filter sets used were as follows: cyan fluorescent protein (CFP), 436/20 nm, 455 nm, 480/40 nm (excitation, beam splitter, emission filter); yellow fluorescent protein (YFP), 500/20 nm, 515 nm, 535/30 nm; and mCherry, 560/40 nm, 585 nm, 630/75 nm (Chroma). Images were acquired every 20 min in the phase and CFP channels and every 60 min in the YFP and mCherry channels. We acquired six z-sections with a step size of 0.75 μm in the YFP and mCherry channels. Image acquisition was controlled by MetaMorph software (Molecular

Devices). This resulted in approximately 5,000–8,000 images per slide, leading to a total of about 100,000 cells. For larger cell counts, data from several slides was concatenated.

Image analysis

Image analysis used Matlab, with an algorithm written by R. Kafri, as described previously[37]. Top-Hat transformation of images was used to remove background trends. Nuclei were identified by thresholding the DAPI image. Boundaries between adjacent, touching nuclei were identified by seed-based watershedding. Seeds were calculated as the regional maxima of the Gaussian smoothed image. Cell boundaries were then found by performing the same steps on the Alexa Fluor 647 scanning electron image using the nuclei as seeds. The integrated immunofluorescence intensity within the cell boundary was taken as the Akt or pS473-Akt amount.

Cdk2/cyclin A *in vitro* kinase assays

Cdk2/cyclin A *in vitro* kinase assay methods were adapted from those described previously[5,31]. Briefly, 3 μg indicated GST–Akt1-Tail (268–480) fusion proteins were incubated with 50 ng commercially obtained recombinant active Cdk2/cyclin A proteins (NEB P6025), in the presence of 5 μCi [γ-^{32}P]ATP and 200 μM cold ATP in the NEB kinase reaction buffer for 30 min. The reaction was stopped by the addition of SDS containing lysis buffer and resolved by SDS–PAGE. Phosphorylation of GST–Akt1-Tail was detected by autoradiography.

For the cold Cdk2/cyclin A *in vitro* kinase assay, no [γ-^{32}P]ATP was added, and the other procedures remained the same. For the *in vitro* kinase assay on full length Akt1, HA-Akt1 was immunoprecipitated from 293T cells and subjected to phosphatase treatment for 30 min at 30 °C before adding into the kinase reaction.

Akt *in vitro* kinase assays

Various HA-Akt1 mutant proteins were HA-immunoprecipitated and stored in EBC buffer with 10% glycerol. Amounts of kinases affinity purified were determined by Coomassie staining. About 2 μg of each kinase was incubated with 50 μM crosstide (Millipore 12-331, based on the Akt phosphorylation site of GSK3), 200 μM ATP (with [γ-^{32}P]ATP) and reaction buffer (50 mM Tris pH 7.5, 1 mM $MnCl_2$, 2 mM DTT, 1 mM EGTA, 1 mg ml^{-1} BSA) at 30 °C for 1 h. Aliquots of each reaction were spotted onto P81 phosphocellulose filters and washed extensively with 75 mM phosphoric acid. Filters were dried and radioactivity was determined by scintillation counting. Experiments were done in triplicate.

To test the ability of peptides based on the hydrophobic motif of Akt2 to activate the enzyme, the activity of pΔPH-Akt2-ΔC (Akt2 lacking the PH domain and C-terminal tail (residues 146–460) but phosphorylated on T309 by GST–PDK1, as described in ref. 23) was determined in the presence of various hydrophobic-motif peptides. pΔPH-Akt2-ΔC (50 nM) was combined with 50 mM substrate peptide (crosstide, based on the Akt phosphorylation site of GSK3), 500 μM ATP (with [γ-^{32}P]ATP), hydrophobic-motif peptides and buffer (50 mM Tris pH 7.5, 10 mM $MgCl_2$, 2 mM DTT, 1 mM EGTA, 1 mg ml^{-1} BSA) at 30 °C for 1 h. Aliquots of each reaction were spotted onto P81 phosphocellulose filters and washed

extensively with 75 mM phosphoric acid. Filters were dried and radioactivity was determined by scintillation counting. Experiments were done in triplicate.

mTOR *in vitro* kinase assay on peptide libraries

The reaction contained 100 ng mTOR (EMD/Calbiochem 475987, containing truncated mTOR kinase domain with amino acids 1,360–2,549), 50 mM biotinylated peptide mix and 100 μM cold ATP (with 0.8 μCi/ml^{-1} [γ-^{32}P]ATP) in assay buffer (50 mM HEPES pH 7.5, 10 mM $MnCl_2$, 10 mM $MgCl_2$, 2 mM DTT, 0.5 mM EGTA). In each biotinylated peptide mix, one amino acid is fixed at the indicated position relative to a central serine/threonine residue. The remaining positions surrounding the central serine/threonine are degenerate (approximately equimolar mixtures of the 17 amino acids excluding cysteine, serine and threonine). The reactions were at 30 °C for approximately 7 h. Aliquots of each reaction were then spotted onto an avidin-coated membrane. The membrane was washed sequentially with 0.1% SDS in TBS, 1% H_3PO_4 and 2 M NaCl. After washing, the membrane was dried and exposed to a phospho-imager. The extent of incorporation of radiolabelled phosphate into each peptide was quantified using ImageQuant software.

Mass spectrometry analysis to detect HA-Akt-S477/T479 phosphorylation *in vivo*

The procedures of mass spectrometry analysis were performed as described previously[40,41] with minor modifications. Briefly, 293 cells were transiently transfected with the pcDNA3-HA-Akt1 plasmid and, 24 h after transfection, cells were treated with insulin for 30 min before collection. Whole-cell lysates were collected to perform HA immunoprecipitation. The HA immunoprecipitates were then resolved on SDS–PAGE and visualized by colloidal Coomassie blue. The band containing HA-Akt1 was excised and washed with 50% acetone. In-gel digestion of the protein was performed with trypsin and analysed by reversed-phase microcapillary/tandem mass spectrometry using a LTQ Orbitrap XL (Thermo Fisher Scientific) Hybrid Ion Trap-Orbitrap Mass Spectrometer. Tandem mass spectrometry centroid spectra collected by collision-induced dissociation in Top 6 data-dependent acquisition mode were searched against the concatenated target and decoy(reversed) Swiss-Prot protein database (version 2012_01) using the Sequest search engine with Proteomics Browser Software (W.S. Lane) with differential modifications for Ser/Thr/Tyr phosphorylation (+79.97) and differential modification of Met oxidation (+15.99, Msx). Phosphorylated and unphosphorylated peptide sequences were identified, and manual inspection and determination of the exact sites of phosphorylation were confirmed using FuzzyIons and GraphMod software (Proteomics Browser Software, W.S. Lane). False discovery rates of peptide hits (phosphorylated and non-phosphorylated) were estimated below 1.0% based on reversed database hits.

Mass spectrometry analysis to detect GST–Akt-S477/T479 phosphorylation *in vitro*

The mass spectrometry procedure was performed as described previously[40,41]. Phosphorylated GST–Akt1 samples were prepared as described in the kinase assay section, with Cdk2/cyclin A or mTOR, respectively. Specifically, 1 μg of phosphorylated HA-Akt1 proteins were subjected to trypsin digestion before being analysed by mass spectrometry.

5-Bromodeoxyuridine labelling

5-Bromodeoxyuridine labelling assay was performed as described previously[32]. Experiments were repeated three times to generate the error bars.

Soft agar assay

The anchorage-independent cell growth assays were performed as described previously[42]. The solid medium consists of two layers. The bottom layer contains 0.8% noble agar and the top layer 0.4% agar. Briefly, 3×10^5 cells were plated in the top layer. Complete DMEM medium (500 μl) was added every other day to keep the top layer moisture, and 3 weeks later the cells were stained with iodonitrotetrazolium chloride for colony visualization and counting. Three independent experiments were performed to generate the error bars.

Mouse xenograft assay

The tumorigenesis assay was as described previously[43]. Each xenograft experiment was performed as described in the corresponding figure legends. For example, in Fig. 4f, g, briefly 2.5×10^6 HeLa cells stably expressing HA-Akt1-WT, HA-Akt1-S477A/T479A or HA-Akt1-S477D/T479E (using empty vector as a negative control) were mixed with sterile 1× PBS (1:1) and injected into the flank of 10 male nude mice. Tumour size was measured weekly with a calliper, and the tumour volume was determined with the formula $L \times W^2 \times 0.52$, where L is the longest diameter and W is the shortest diameter. After 28 days, mice were killed and *in vivo* solid tumours were dissected, then tumour weights were measured and recorded.

Immunohistochemistry of tissue microarray (immunohistochemistry and immunostaining analyses)

Formalin-fixed and paraffin-embedded tissue microarrays of human breast tissues and breast cancer tissues were purchased from Imgenex (IMH-371). Immunohistochemical stainings for cyclin A2, Akt-pS473 and Akt-pS477/pT479 were performed as described previously[44]. The cyclin A2 antibody for immunohistochemistry was purchased from Santa Cruz (sc-751), Akt-pS473 antibody for immunohistochemistry was purchased from Cell Signaling Technology (4060) and the Akt-pS477/pT479 antibody was generated by collaboration with the Cell Signaling Technology and further validated in this study.

Generation of cyclin $A2^{f/f}$ nestin-Cre mice, and brain tissue analysis

Olfactory bulbs, cortices and cerebella from cyclin $A2^{flox/flox}$ nestin-Cre mice[45], obtained by crossing cyclin $A2^{flox/+}$ mice with nestin-Cre mice, were collected on the postnatal day 2, lysed and analysed by immunoblots.

Generation of Akt1 expressing cyclin $A1^{-/-}$/cyclin $A2^{f/f}$/Cre-ER mouse embryonic stem cell lines

cyclin $A1^{-/-}$/cyclin $A2^{flox/flox}$ mouse embryonic stem cells[14] were electroporated with the pMSCV-CreER-puro expressing vector and then plated on a monolayer of arrested, puromycin-resistant feeder fibroblasts. After 2 days, cells were subjected to selection by 2 μg ml^{-1} puromycin until resistant colonies became apparent (about 7 days). Single colonies

were picked, expanded and tested for Cre-ER expression by immunoblot analysis. The resulting cells were infected with pBabe-hygro-HA-Akt1-DE or -AA retroviruses (using pBabe-hygroempty vector as a negative control) and selected in 1 μg ml^{-1} puromycin in combination with 250 ng ml^{-1} hygromycin for 3 days to eliminate non-infected cells and tested for Akt1 expression by HA immunoblot analysis.

Supplementary Material

Refer to Web version on PubMed Central for supplementary material.

Acknowledgments

We thank J. Guo, J.J. Liu, A.W. Lau, S. Shaik, A. Tron, X. Dai and K. Xu for reading the manuscript, S.B. Breitkopf for help with mass spectrometry experiments, Y. Geng, L. Liu, K. Ran, R. Chin and S. Elloul for providing reagents, and members of the Wei, Toker, Sicinski, Pandolfi and Cantley laboratories for discussions. W.W. is an American Cancer Society and a Leukemia & Lymphoma Society research scholar. P.L. is supported by 5T32HL007893. This work was supported in part by National Institutes of Health grants to W.W. (GM089763, GM094777 and CA177910), J.M.A. (2P01CA120964) and P.S. (R01CA132740).

References

1. Zoncu R, Efeyan A, Sabatini DM. mTOR: from growth signal integration to cancer, diabetes and ageing. Nature Rev. Mol. Cell Biol. 2010; 12:21–35. [PubMed: 21157483]
2. Manning BD, Cantley LC. AKT/PKB signaling: navigating downstream. Cell. 2007; 129:1261–1274. [PubMed: 17604717]
3. Toker A. Akt signaling: a damaging interaction makes good. Trends Biochem. Sci. 2008; 33:356–359. [PubMed: 18585043]
4. Luo J, Manning BD, Cantley LC. Targeting the PI3K-Akt pathway in human cancer: rationale and promise. Cancer Cell. 2003; 4:257–262. [PubMed: 14585353]
5. Sarbassov DD, Guertin DA, Ali SM, Sabatini DM. Phosphorylation and regulation of Akt/PKB by the rictor-mTOR complex. Science. 2005; 307:1098–1101. [PubMed: 15718470]
6. Stephens L, et al. Protein kinase B kinases that mediate phosphatidylinositol 3,4,5-trisphosphate-dependent activation of protein kinase B. Science. 1998; 279:710–714. [PubMed: 9445477]
7. Hanahan D, Weinberg RA. Hallmarks of cancer: the next generation. Cell. 2011; 144:646–674. [PubMed: 21376230]
8. Gao X, Zhang J. Spatiotemporal analysis of differential Akt regulation in plasma membrane microdomains. Mol. Biol. Cell. 2008; 19:4366–4373. [PubMed: 18701703]
9. Sakaue-Sawano A, et al. Visualizing spatiotemporal dynamics of multicellular cell-cycle progression. Cell. 2008; 132:487–498. [PubMed: 18267078]
10. McGarry TJ, Kirschner MW. Geminin, an inhibitor of DNA replication, is degraded during mitosis. Cell. 1998; 93:1043–1053. [PubMed: 9635433]
11. Murphy M, et al. Delayed early embryonic lethality following disruption of the murine cyclin A2 gene. Nature Genet. 1997; 15:83–86. [PubMed: 8988174]
12. Maddika S, et al. Akt-mediated phosphorylation of CDK2 regulates its dual role in cell cycle progression and apoptosis. J. Cell Sci. 2008; 121:979–988. [PubMed: 18354084]
13. Adams PD, et al. Identification of a cyclin-cdk2 recognition motif present in substrates and p21-like cyclin-dependent kinase inhibitors. Mol. Cell. Biol. 1996; 16:6623–6633. [PubMed: 8943316]
14. Kalaszczynska I, et al. Cyclin A is redundant in fibroblasts but essential in hematopoietic and embryonic stem cells. Cell. 2009; 138:352–365. [PubMed: 19592082]
15. Geley S, et al. Anaphase-promoting complex/cyclosome-dependent proteolysis of human cyclin A starts at the beginning of mitosis and is not subject to the spindle assembly checkpoint. J. Cell Biol. 2001; 153:137–148. [PubMed: 11285280]

16. Malumbres M, Barbacid M. Mammalian cyclin-dependent kinases. Trends Biochem. Sci. 2005; 30:630–641. [PubMed: 16236519]
17. Gray CH, Barford D. Getting in the ring: proline-directed substrate specificity in the cell cycle proteins Cdc14 and CDK2-cyclinA3. Cell Cycle. 2003; 2:500–502. [PubMed: 14504459]
18. Liu P, Kenney JM, Stiller JW, Greenleaf AL. Genetic organization, length conservation, and evolution of RNA polymerase II carboxyl-terminal domain. Mol. Biol. Evol. 2010; 27:2628–2641. [PubMed: 20558594]
19. Stokes MP, et al. PTMScan direct: identification and quantification of peptides from critical signaling proteins by immunoaffinity enrichment coupled with LC-MS/MS. Mol. Cell. Proteom. 2012; 11:187–201.
20. Bozulic L, Surucu B, Hynx D, Hemmings BA. PKBα/Akt1 acts downstream of DNA-PK in the DNA double-strand break response and promotes survival. Mol. Cell. 2008; 30:203–213. [PubMed: 18439899]
21. Xie X, et al. IκB kinase epsilon and TANK-binding kinase 1 activate AKT by direct phosphorylation. Proc. Natl Acad. Sci. USA. 2011; 108:6474–6479. [PubMed: 21464307]
22. Yang J, et al. Crystal structure of an activated Akt/protein kinase B ternary complex with GSK3-peptide and AMP-PNP. Nature Struct. Biol. 2002; 9:940–944. [PubMed: 12434148]
23. Yang J, et al. Molecular mechanism for the regulation of protein kinase B/Akt by hydrophobic motif phosphorylation. Mol. Cell. 2002; 9:1227–1240. [PubMed: 12086620]
24. Alessi DR, Pearce LR, Garcia-Martinez JM. New insights into mTOR signaling: mTORC2 and beyond. Sci. Signal. 2009; 2:27.
25. Maira SM, et al. Carboxyl-terminal modulator protein (CTMP), a negative regulator of PKB/Akt and v-Akt at the plasma membrane. Science. 2001; 294:374–380. [PubMed: 11598301]
26. Gao T, Furnari F, Newton AC. PHLPP: a phosphatase that directly dephosphorylates Akt, promotes apoptosis, and suppresses tumor growth. Mol. Cell. 2005; 18:13–24. [PubMed: 15808505]
27. Gaveriaux-Ruff C, Kieffer BL. Conditional gene targeting in the mouse nervous system: Insights into brain function and diseases. Pharmacol. Ther. 2007; 113:619–634. [PubMed: 17289150]
28. Burgess DJ. Senescence: double or quit? Nature Rev. Cancer. 2011; 11:389. [PubMed: 21562582]
29. Butt AJ, et al. Cell cycle machinery: links with genesis and treatment of breast cancer. Adv. Exp. Med. Biol. 2008; 630:189–205. [PubMed: 18637492]
30. Altomare DA, Testa JR. Perturbations of the AKT signaling pathway in human cancer. Oncogene. 2005; 24:7455–7464. [PubMed: 16288292]
31. Gao D, et al. Phosphorylation by Akt1 promotes cytoplasmic localization of Skp2 and impairs APCCdh1-mediated Skp2 destruction. Nature Cell Biol. 2009; 11:397–408. [PubMed: 19270695]
32. Gao D, et al. Cdh1 regulates cell cycle through modulating the claspin/Chk1 and the Rb/E2F1 pathways. Mol. Biol. Cell. 2009; 20:3305–3316. [PubMed: 19477924]
33. Wei W, et al. Degradation of the SCF component Skp2 in cell-cycle phase G1 by the anaphase-promoting complex. Nature. 2004; 428:194–198. [PubMed: 15014503]
34. Peng XD, et al. Dwarfism, impaired skin development, skeletal muscle atrophy, delayed bone development, and impeded adipogenesis in mice lacking Akt1 and Akt2. Genes Dev. 2003; 17:1352–1365. [PubMed: 12782654]
35. Silva JM, et al. Second-generation shRNA libraries covering the mouse and human genomes. Nature Genet. 2005; 37:1281–1288. [PubMed: 16200065]
36. Tsou P, Zheng B, Hsu CH, Sasaki AT, Cantley LC. A fluorescent reporter of AMPK activity and cellular energy stress. Cell Metab. 2011; 13:476–486. [PubMed: 21459332]
37. Karanam K, Kafri R, Loewer A, Lahav G. Quantitative live cell imaging reveals a gradual shift between DNA repair mechanisms and a maximal use of HR in mid S phase. Mol. Cell. 2012; 47:320–329. [PubMed: 22841003]
38. Dean PN, Jett JH. Mathematical analysis of DNA distributions derived from flow microfluorometry. J. Cell Biol. 1974; 60:523–527. [PubMed: 4855906]
39. Toettcher JE, et al. Distinct mechanisms act in concert to mediate cell cycle arrest. Proc. Natl Acad. Sci. USA. 2009; 106:785–790. [PubMed: 19139404]

40. Gao D, et al. Rictor forms a complex with Cullin-1 to promote SGK1 ubiquitination and destruction. Mol. Cell. 2010; 39:797–808. [PubMed: 20832730]

41. Inuzuka H, et al. Phosphorylation by casein kinase I promotes the turnover of the Mdm2 oncoprotein via the SCF(β-TRCP) ubiquitin ligase. Cancer Cell. 2010; 18:147–159. [PubMed: 20708156]

42. Wei W, Jobling WA, Chen W, Hahn WC, Sedivy JM. Abolition of cyclin-dependent kinase inhibitor p16Ink4a and p21Cip1/Waf1 functions permits Ras-induced anchorage-independent growth in telomerase-immortalized human fibroblasts. Mol. Cell. Biol. 2003; 23:2859–2870. [PubMed: 12665584]

43. Inuzuka H, et al. Acetylation-dependent regulation of Skp2 function. Cell. 2012; 150:179–193. [PubMed: 22770219]

44. Min SH, et al. Negative regulation of the stability and tumor suppressor function of fbw7 by the pin1 prolyl isomerase. Mol. Cell. 2012; 46:771–783. [PubMed: 22608923]

45. Otero JJ, et al. Cerebellar cortical lamination and foliation require cyclin A2. Dev. Biol. 2014; 385:328–339. [PubMed: 24184637]

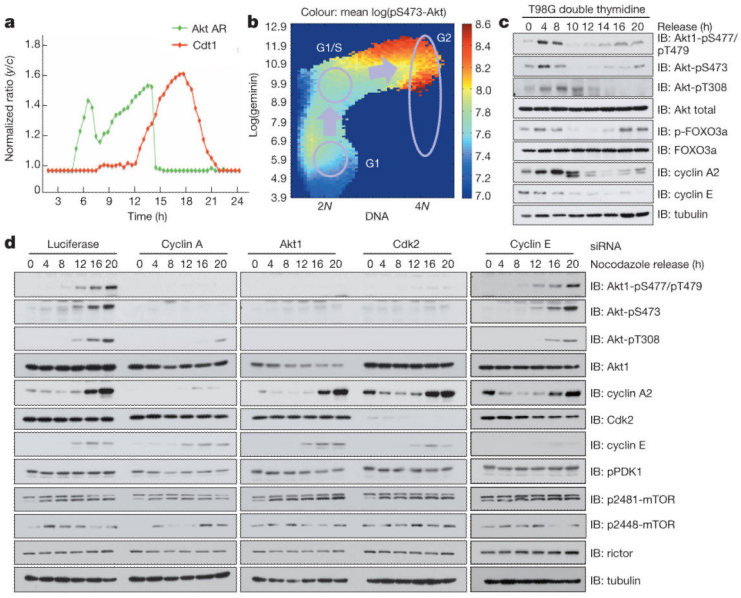

Figure 1. Akt activity fluctuated during the cell cycle and mirrored the periodic cyclin A expression pattern

a, Single live-cell imaging of the Akt activity reporter (green, EGFP–Akt AR (activity reporter)) and the cell cycle marker Cdt1 (red, mCherry–Cdt1) transiently expressed in non-synchronized HeLa cells. **b,** A representative heat map of cell-cycle-dependent Akt1-pS473 as a function of DNA content (*x* axis) and geminin expression as an indicator of cell cycle stages (*y* axis). Blue, low Akt-pS473; red, high Akt-pS473. Number of cells was more than 500. **c,** Akt phosphorylation fluctuated across the cell cycle. Immunoblot (IB) of whole-cell lysates (WCLs) derived from T98G cells synchronized by double thymidine block and released to normal cell cycle for the indicated periods. **d,** Depletion of cyclin A, but not cyclin E, led to reduced Akt phosphorylation across the cell cycle. Immunoblot of whole-cell lysates derived from HeLa cells synchronized by nocodazole and released for the indicated periods. Where indicated, short interfering RNA (siRNA) oligonucleotides were transfected into cells 24 h before synchronization.

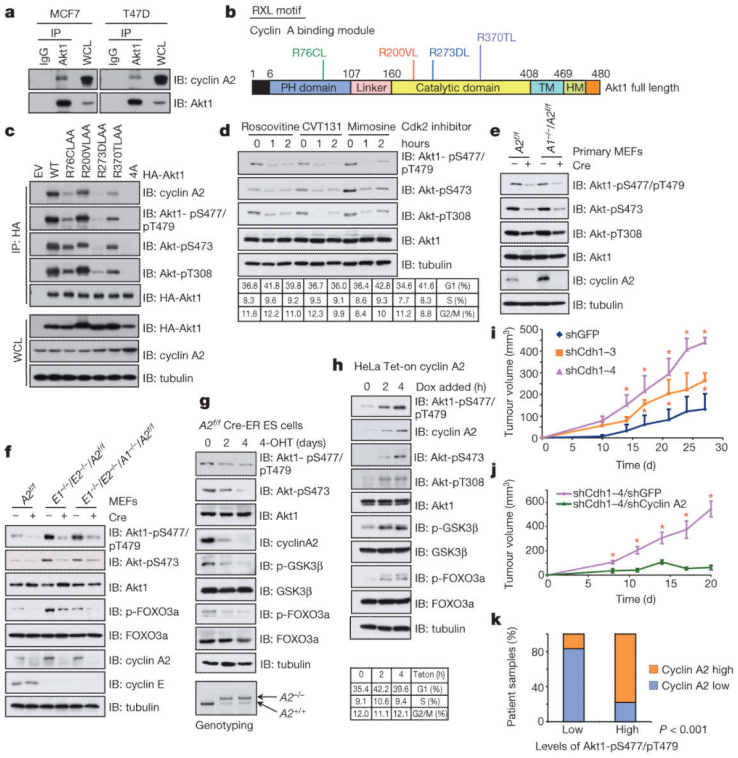

Figure 2. Cdk2/cyclin A2 functioned as a physiological kinase phosphorylating Akt1 at both S477 and T479

a, Akt1 interacted with cyclin A2 at endogenous levels. Immunoblot analysis of WCLs and anti-Akt1 immunoprecipitations (IP) derived from MCF7 or T47D cells. **b,** Illustration of four putative cyclin A binding motifs (RXL) in human Akt1. **c,** Deficiency in cyclin A binding led to attenuated Akt phosphorylation. Immunoblot of WCLs and human influenza hemagglutinin (HA)-immunoprecipitations derived from HeLa cells transfected with indicated HA-Akt1 constructs. **d,** Immunoblot of WCLs derived from HeLa cells treated with indicated Cdk2 inhibitors at various time points. Drug doses used were roscovitine (40 μM), CVT-131 (0.5 μM) and mimosine (50 μM). **e,** Immunoblot of WCLs derived from cyclin $A2^{f/f}$ primary MEFs with or without adenoviral-Cre infection. **f,** Immunoblot of WCLs derived from indicated immortalized MEFs with or without Cre viral infection. **g,** Immunoblot of WCLs derived from cyclin $A2^{f/f}$ mouse embryonic stem (ES) cells stably expressing Cre-ER treated with 2 μg ml^{-1} tamoxifen (4-OHT) for the indicated days. **h,** Immunoblot of WCLs derived from HeLa cells stably expressing inducible pTRIPZ-cyclin-A2 treated with 500 ng ml^{-1} doxycycline for the indicated periods. **i, j,** MDA-MB-231 cells depleted of Cdh1 by two independent shRNAs (**i**), or depleted of both Cdh1 and cyclin A2 (**j**), were injected into nude mice (n = 10 for each group) and monitored for tumorigenesis *in vivo*. *$P < 0.05$ (Student's t-test). **k,** Relative percentages of 50 samples examined from patients with breast cancer bearing the indicated cyclin A2 and Akt1-pS477/pT479 status indexed by either low or high.

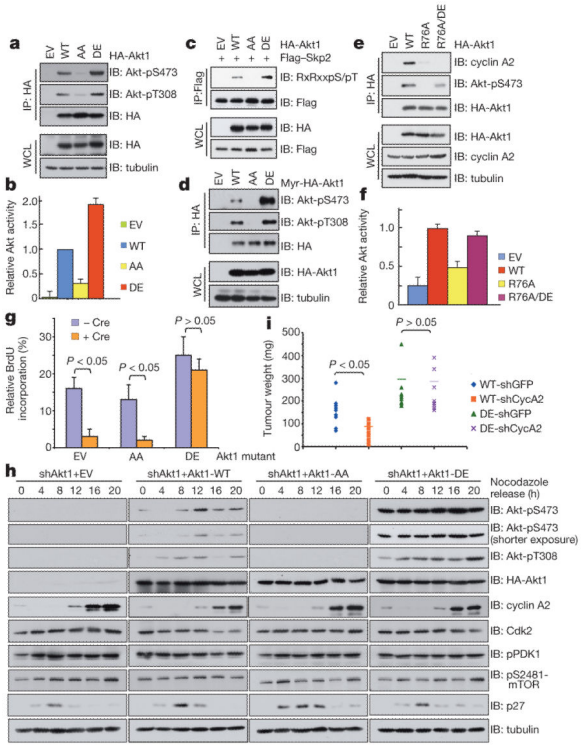

Figure 3. Akt1-S477/T479 phosphorylation triggered Akt1-S473 phosphorylation and enhanced Akt1 activation

a, Akt1-S477D/T479E mutation led to elevated Akt-pS473. Immunoblot of WCLs and HA-immunoprecipitations derived from HeLa cells transfected with indicated Akt1 constructs. EV, empty vector. **b,** *In vitro* kinase assays of indicated affinity-purified Akt1 kinases with crosstide as a substrate. Experiments were performed in triplicate; data are shown as mean ± s.d. **c,** Akt1-S477D/T479E mutation resulted in enhanced Skp2 phosphorylation. Immunoblot of WCLs and Flag-immunoprecipitations derived from HeLa cells transfected with indicated Akt1 constructs together with Flag–Skp2. **d, e,** Immunoblot of WCLs and HA-immunoprecipitations derived from HeLa cells transfected with indicated Akt1 constructs. **f,** *In vitro* kinase assays of indicated affinity-purified Akt1 kinases with crosstide as a substrate. Experiments were performed in triplicate; data are shown as mean ± s.d. **g,** Relative 5-bromodeoxyuridine (BrdU) incorporation for quadruple knockout MEFs (cyclin $E1^{-/-}$/ $E2^{-/-}$/$A1^{-/-}$/$A2^{f/f}$) expressing indicated Akt1 constructs that were further infected with or without Cre to delete the cyclin A2 alleles. **h,** Akt1-S477D/T479E mutation led to sustained Akt phosphorylation across the cell cycle. Immunoblot of WCLs derived from HeLa cells transfected with indicated Akt1 constructs, synchronized by nocodazole and released for indicated periods. **i,** Akt1-depleted HeLa cells stably expressing Akt1-WT or -DE were subcutaneously injected into nude mice (n = 10 for each group) and monitored for tumorigenesis. P values were calculated by Student's t-test.

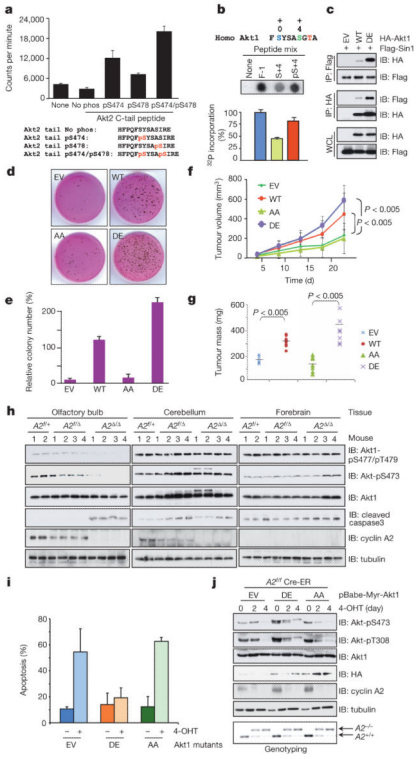

Figure 4. Akt tail phosphorylation triggered Akt activation to promote Akt oncogenic functions

a, Stimulation of purified recombinant pΔPH-Akt2-ΔC kinase activity by indicated Akt2 C-terminal tail peptides. pΔPH-Akt2-ΔC, Akt2 residues 146–460, lacking the PH domain and C-terminal tail with T309 phosphorylated. Experiments were performed in triplicate; data are shown as mean ± s.d. No phos, no phosphorylation. **b,** mTOR *in vitro* kinase assays with degenerate peptide libraries as substrates. Experiments were performed in triplicate; data are shown as mean ± s.d. **c,** Akt1-S477D/T479E mutation led to enhanced binding with Sin1. Immunoblot of WCLs and HA- or Flag-immunoprecipitations derived from Akt1-depleted HeLa cells transfected with indicated Akt1 constructs together with Flag–Sin1. **d, e,** Soft agar assays using Akt1-depleted HeLa cells stably expressing WT-, AA- or DE-Akt1. **f, g,** Akt1-depleted HeLa cells stably expressing WT-, AA- or DE-Akt1 were injected subcutaneously into nude mice (n = 10 for each group) and monitored for tumorigenesis (**f**). Tumours were dissected and weighed (**g**). *P < 0.05 (Student's t-test). **h,** Immunoblot analyses of the indicated mouse brain tissues derived from mice with the indicated cyclin A2 genetic status. **i,** Fluorescence-activated cell sorting analysis of cyclin $A2^{f/f}$ mouse embryonic stem cells stably expressing Cre-ER in the presence of 2 μg ml^{-1} tamoxifen for 4 days. **j,** Immunoblot analysis of WCLs derived from various indicated embryonic stem stable cell lines generated in **i**.